Influence of Compaction Conditions on the Foamability of AlSi8Mg4 Alloy

H.-M. HELWIG, S. HILLER, F. GARCIA-MORENO, and J. BANHART

Aluminum AlSi8Mg4 alloy foams were produced by the powder compact foaming route using different parameters for the uniaxial powder compaction step. Compaction time, pressure, and temperature were varied and were found to influence both the density of the foamable precursor and the peak expansion reached during foaming. While peak expansion cannot be related to any single pressing parameter alone in a simple way, a clear dependence of expansion on the precursor density was found. Densification to a relative density between 97.5 and 99 pct yielded volume expansions of the foam up to 880 pct. Lower densities result in weaker foaming, due to insufficient encapsulation of the blowing agent; in addition, we were surprised to find that higher densification also has an adverse effect on peak expansion, most likely due to the elimination of nucleation centers or the effect of entrapped compressed air. Precursor microstructures were analyzed to identify the mechanisms leading to the observed density dependence of expansion.

I. INTRODUCTION

A successful technique to manufacture aluminum-alloy foams is the powder metallurgical (PM) foaming route.[1–3] The foams manufactured in this way are already in small-scale industrial use.[4] The method is comprised of the mixing of metal powders and a blowing-agent powder (usually TiH_2) compacting the mix, and then foaming by melting the compacted precursor.[3]

There are many process parameters that have an influence on foaming, such as the heating rate and foaming temperature,[5,6] the type of blowing agent and its pretreatment before use,[7,8] the alloy composition,[9,10] and the atmospheric composition and pressure during foaming.[11,12]

Among the most important parameters are the compaction conditions of the powder blend. It is surprising that the influence of these has not yet been studied systematically. Reference 5 contains information on the influence of the pressing temperature and pressing time, but not on the variation in pressure that came from a limitation to a maximum pressure of 120 MPa of the hot press used. Reference 13 deals mainly with the influence of powder oxidation during compaction at different temperatures. Reference 14 focuses on the influence of the tool design on the precursor quality for fixed compaction parameters. In the additional literature, compaction "recipes" are presented that yield "good" foam, but parameter optimization is largely poorly documented.

Most of the work done aims at densifying the powder to a threshold density, e.g., 98 pct,[5] in order to sufficiently encapsulate the hydride particles in the matrix and prevent the evolving blowing gas from escaping. Therefore, a density as high as possible is implicitly assumed to be desirable. The parameters that can be varied to achieve densification in a die are the compaction temperature, time, and pressure. The compaction temperature is limited by the decomposition temperature of the blowing agent. Moreover, the hot-working steel used for the tool limits both the temperature and pressure as its strength rapidly decreases upon heating. If uniaxial pressing is applied in mass production, the cost efficiency of the process will strongly depend on the cycle time, putting a practical limitation to the compaction time. In general, cost efficiency can be best achieved by minimizing the compaction time to a value that provides sufficient densification while still being at a temperature and pressure that ensure endurance of the tools.

In industrial practice, the powder blends are primarily compacted by extrusion or rolling.[15] In order to verify that hot pressing can be a viable production technique for a foamable precursor, we investigated the influence of pressure (up to 300 MPa), temperature (up to 500 °C), and pressing time (up to 7000 seconds) on the density and foaming behavior of aluminum-alloy compacts and analyzed their microstructure to explain the effects observed.

H.-M. HELWIG, PhD-Student, Group for Structure and Properties of Materials, Berlin Institute of Technology, is Researcher, Metallic Foam Group, Institute of Materials, Helmholtz-Centre Berlin for Materials and Energy, Berlin, Germany. Contact e-mail: h.helwig@gmx.de S. HILLER, Student, is with the Berlin Institute of Technology, Group for Structure and Properties of Materials. F. GARCIA-MORENO, is Head, Metallic Foam Group of the Institute of Materials, Helmholtz-Centre Berlin for Materials and Energy, and the Metallic Foam Research, Group for Structure and Properties of Materials, Berlin Institute of Technology. J. BANHART, Professor, is Head, Institute of Materials, Helmholtz-Centre Berlin for Materials and Energy, and Group for Structure and Properties of Materials, Berlin Institute of Technology, Berlin, Germany.

II. EXPERIMENTAL

A. Sample Preparation

Alloy AlMg4Si8 was used for the present study of compaction parameters, because the corresponding powder mixture, comprised of ductile and brittle components, was expected to be difficult to consolidate and show clear effects of insufficient consolidation. On the other hand, it has already been established that this type of alloy can be foamed in a satisfactory way.[10] The overall alloy composition was realized by mixing various powders in the fractions given in Table I in a tumbling mixer. The mixture contained a 1 mass pct TiH_2 powder that had been heat treated in air for 3 hours at 480 °C to delay hydrogen evolution.[8]

Cylindrical precursor material tablets, 36 mm in diameter, 7-mm high, and weighing 20 g, were produced by uniaxial hot pressing with varied compaction pressure, time, and temperature. The pressing tool consisted of a cylindrical die and two punches, both made of 1.2344 (DIN EN 10027, Helmholtz-Centre Berlin for Materials and Energy, Berlin, Germany) hot-working steel. The die was surrounded by a heating belt. A thermocouple fitted into a hole in the die provided the signal for the heating controller. The risk of embrittlement for this steel[16] was the reason for limiting the compaction temperature to, in general, 400 °C, although a few exceptions were made to examine more extended parameter sets, which allows for a comparison with other studies. Axial pressures ranged from 100 to 300 MPa.

To produce precursors, the cold die was filled with the powder blend, which was then precompacted for 1 second at the same pressure to be applied for hot compaction. After this, the tool was heated to the hot pressing temperature, taking typically 30 minutes. Hot compaction at temperatures up to 400 °C lasted routinely up to 15 minutes. In addition, a few longer compactions were carried out, to get closer to the maximum achievable densification. After compaction, the tool was cooled in cold water and the precursor was removed. Altogether, 61 parameter variations were studied.

B. Density Measurement

The density of the precursor tablets was measured by Archimedes' principle, using a Sartorius BP211D (Sartorius AG, Göttingen, Germany) balance. Ethanol with a tenside addition to decrease surface tension effects was used as buoyant.

C. Expansion Measurement

To measure foam expansion, a special dilatometer (a so-called "expandometer") designed for *in-situ* metal foam expansion measurements by the Institute of Materials and Machine Mechanics of the Slovak Academy of Sciences (Bratislava 3, Slovak republic) was used. It consists of an infrared furnace and a cylindrical mold open only at the top, to accommodate a movable piston connected to a position sensor that monitors foam expansion. For a more detailed description of the method and a comparison with alternative methods, refer to Reference 10. In our case, we wanted to measure peak expansion. For this, the sample was heated with a reproducible and constant linear temperature ramp of $2~Ks^{-2}$. This is important because previous investigations showed an influence of heating rate on foam expansion.[6,17] After heating to 630 °C, the temperature was kept stable for 5 minutes, to ensure that the foaming process could be completed.

D. Microscopy

Three unfoamed samples were selected for further microscopic investigations. The samples were made by applying different compaction parameters; all have a different foaming behavior.

In order to examine the bonding between powder particles after pressing, fracture surfaces were prepared by breaking thin slices of precursor material. To avoid plastic deformation during fracture, the samples were immersed in liquid nitrogen before breaking. The fracture surfaces were observed with a PHILIPS* XL-30

---

*PHILIPS is a trademark of Philips Electronic Instruments Corp., Mahwah, NJ.

ESEM scanning electron microscope (SEM).

To quantify the residual porosity in the compacted powder blend, cut surfaces were prepared. Unlike in normal metallographic preparation, the polishing steps after grinding were omitted and replaced by grinding with papers down to a 1-μm particle size, because polishing with soft polishing compound carriers was found to lead to edge-rounding of the soft aluminum particles and to closure of small pores. The SEM images were analyzed using the free image-analysis software ImageTool[18] (UTHSCSA Dental Diagnostic Science, San Antonio, TX) to count and classify the pores according to their size.

Table I. Powders Used for Foam Manufacture; Purity as Specified by Supplier; Grain Size Parameters D_{xx} Measured with Sympatec Helos Laser Diffractometer (Sympatec GmbH, System-Partikel-Technik, Clausthal-Zellerfeld, Germany) (AlMg7.8 Contains Particles outside the Measurable Range); Last Column Gives Mass Fraction in AlSi8Mg4 + TiH_2 Powder Blend

Type	Supplier	Purity (Mass Pct)	D_{10} (μm)	D_{50} (μm)	D_{90} (μm)	Fraction (Mass Pct)
Al	Alpoco Ltd. (Sutton Coldfield, UK)	99.7	16.4	38.2	75.5	39.8
AlMg7.8	Possehl Erzkontor GmbH (Lübeck, Germany)	n.sp.	>14.4	>65.1	135.6	51.3
Si	Elkem ASA (Oslo, Norway)	99.5	7.0	25.2	50.0	7.9
TiH_2	Chemetall GmbH (Frankfurt, Germany)	98.3	3.2	14.4	34.2	1.0

n.sp. not specified.

High-resolution imaging was done using a Zeiss Gemini** FIB 1540 ESB SEM. Surfaces were ion

---

**Gemini is a Trademark of Carl Zeiss NTS GmbH, Oberkochen, Germany.

---

milled using a Baltec RES 100 (BAL-TEC AG, Balzers, Principality of Liechtenstein), in this case. We studied microcracks and particle fracture qualitatively.

III. RESULTS

A. *Precursor Density*

All the relative densities given in this study refer to the maximum achievable "full" density reached by hot compaction at 400 °C and 300 MPa. To determine this density, experiments with increasing densification times were carried out. A density increase with time up to 1 hour is observed, after which no notable further increase in density took place. The value for 1 hour was accepted as the full density (Figure 1).

Alternatively, the bulk density can be calculated. Problems include the unknown oxide type and the content of the powders and their limited purity. Alumina and most impurities (*e.g.*, the estimated 0.2 mass pct of iron) increase the density of the alloy. Another source for uncertainty is that the exact bulk density of the AlMg master alloy used has to be extrapolated from other alloy data[10] and that TiH_2 undergoes a slight density change during heat treatment. In Figure 1, the calculated bulk density is given as a function of the alumina content. Additional oxides such as spinel and impurities were not taken into account. The highest measured density value matches the calculated bulk density for ≈0.7 mass pct alumina content (≈0.33 mass

pct oxygen content), a value that is plausible for air-atomized powders (discussion in Reference 19). We therefore use the value 2.632 gcm^{-3} as a good approximation for the full density.

B. *Measurement of Foam Expansion*

In Figure 2, the expansion and temperature course of three foaming experiments are given. These experiments were carried out with precursor tablets made under identical conditions. The temperature curves show the good reproducibility of the temperature ramp used for heating, except for a small temperature regime in which the proportional integral differential (PID) temperature controller produced a slight overheating effect when switching from a constant heating rate to a constant temperature at 630 °C.

Foam expansion was continuous, reaching a peak value after which a slight foam collapse was observed that was followed by a regime of constant volume reading. The expansion values used in this study were taken from the peak values as marked in Figure 2. They were corrected for the thermal expansion of the system expressed by the slope of the expansion curves before the onset of foaming. The zero point of expansion is defined as shown in Figure 2. The varying peak values reflect the usual scatter in such experiments.

C. *Peak Expansion as a Function of Compaction Parameters*

In Figure 3(a), the maximum expansions reached for precursors compacted at 300 °C and at different pressures are given as a function of the compaction time. For the intermediate pressures 150 and 200 MPa and for compaction times up to ≈300 seconds, a significant increase in peak expansion with compaction time is observed, whereas for the highest and lowest compaction pressures, the pressing time hardly influences peak expansion. For a 300-MPa compaction pressure, foamability was always excellent; for 100 MPa, it was always poor.
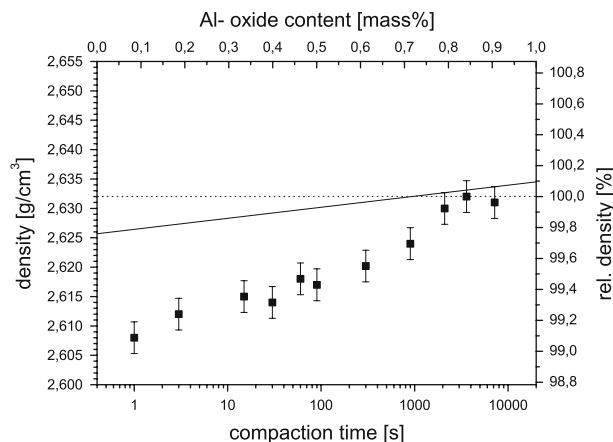

Fig. 1—Experimental determination of full density by varying compaction time, while compaction temperature was 400 °C and pressure 300 MPa (squares, lower axis). A theoretical density calculation based on varying aluminum oxide contents is also included (full line, top axis). Densities for the alloy and oxide used are 2.626 and 3.94 gcm^{-3}, respectively. Horizontal dotted line is the value for full density accepted for this article.
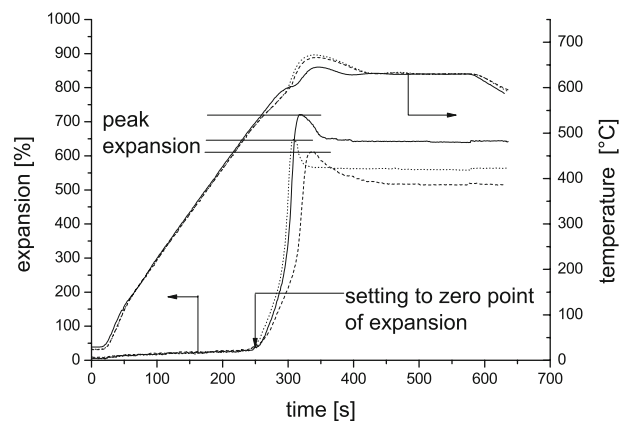

Fig. 2—Expansion and temperature course for three experiments based on precursors made with identical compaction parameters (300 MPa, 900 s, 400 °C).
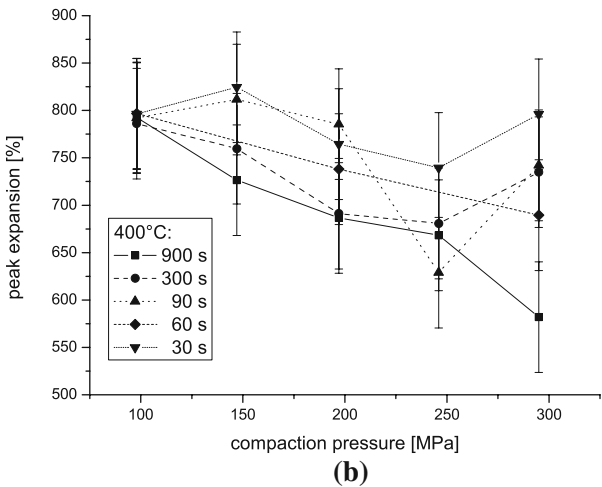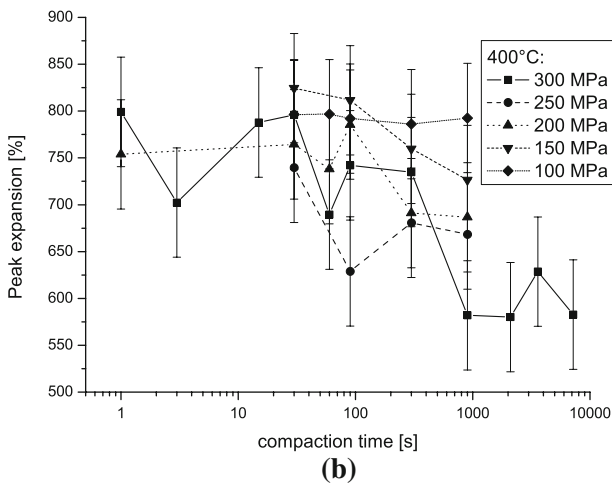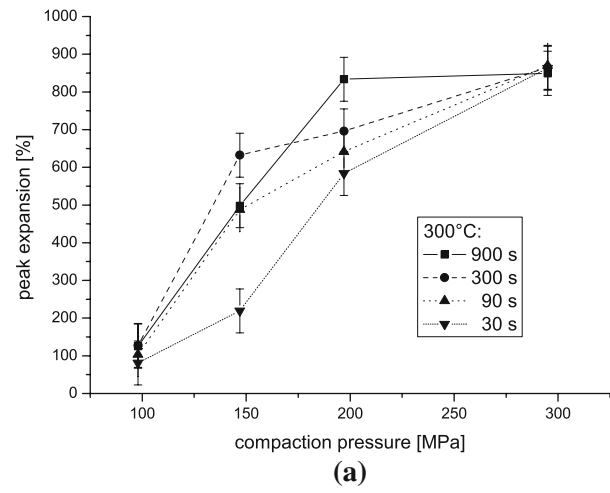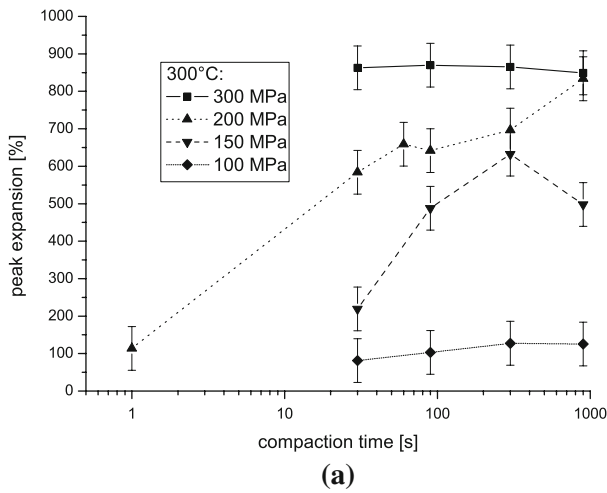
Fig. 3—(a) Peak expansion as a function of compaction time for 300 °C compaction temperature and four different compaction pressures. (b) Same for 400 °C compaction temperature and five different compaction pressures. Note that the expansion scale in (b) is magnified compared to (a).

Fig. 4—(a) Peak expansion as a function of compaction pressure for 300 °C compaction temperature and four different compaction times. (b) Same for 400 °C compaction temperature and five different compaction times. Note that the expansion scale in (b) is magnified compared to (a). All 16/23 values in (a) and (b) are also contained in Figs. 3(a) and (b).

For a 400 °C compaction temperature (Figure 3(b)), the picture is different. Now, longer compaction times can lead to smaller peak expansions. This happens especially for the highest pressure of 300 MPa, at which peak expansion goes down from ≈800 to ≈600 pct with increasing pressing time. Moreover, the lowest pressures, 100 and 150 MPa, lead to peak expansions for all the compaction times studied that were higher than the highest pressures. For 100 MPa, the compaction time does not influence peak expansion. The other compaction pressures fit in between these two extreme cases. It is worth noting that 1 second of compaction at 300 MPa is sufficient to produce ≈800 pct foam expansion. A major difference between the compaction at 300 °C and 400 °C is the range of achieved expansion values. For 300 °C, peak expansion varies from 81 to 870 pct, i.e., the span from a nearly unfoamable precursor to a precursor with excellent foaming behavior, whereas for 400 °C, peak expansions range from just 580 to 825 pct,

i.e., good to excellent foam expansion is achieved in all cases.

Figure 4 displays some of the data given in Figure 3 as a function of the compaction pressure. For a 300 °C compaction temperature and compaction times between 30 and 900 seconds (Figure 4(a)), the peak expansion values increase with the compaction pressure for all compaction times studied and range from ≈100 pct for a 100-MPa compaction pressure up to ≈860 pct for a 300-MPa compaction pressure, with a large scatter at the intermediate compaction pressures of 150 and 200 MPa. For a 400 °C compaction temperature (Figure 4(b)), peak expansion decreases with the compaction pressure, especially for a 900-second compaction time. For shorter compaction times, the decrease is smaller and is not monotonic.

Peak expansions as a function of the compaction temperature for a 300-second compaction time and different compaction pressures are given in Figure 5(a).
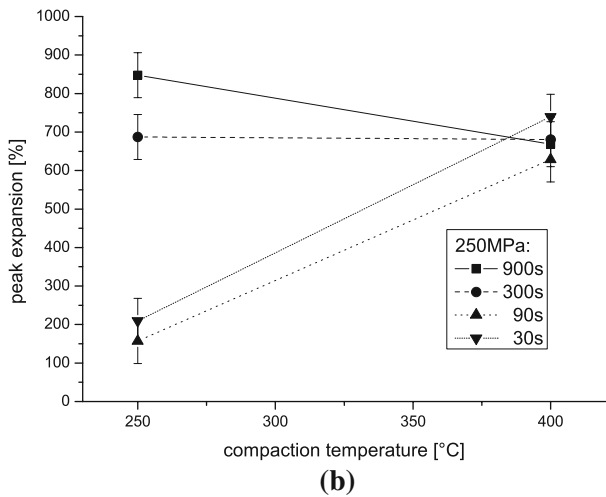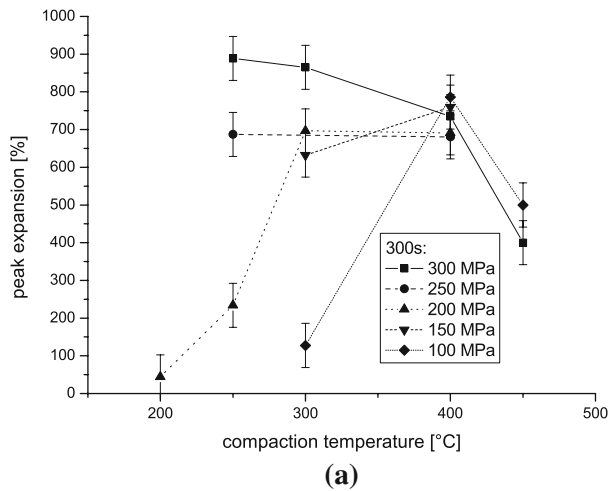
Fig. 5—(a) Peak expansion as a function of compaction temperature measured for five different compaction pressures and 300-s compaction time. (b) Same for four different compaction times and 250-MPa compaction pressure.
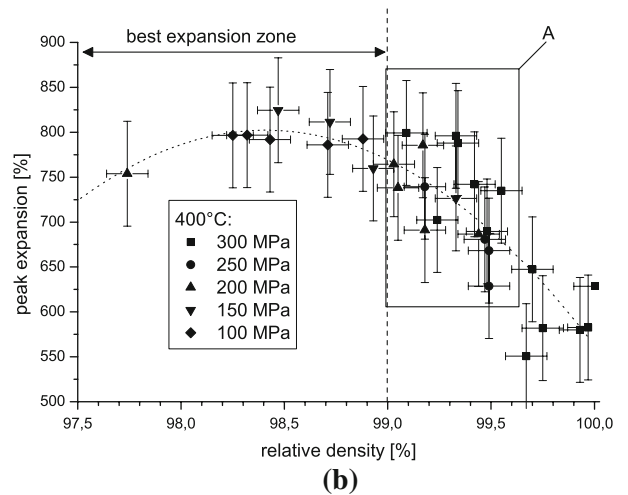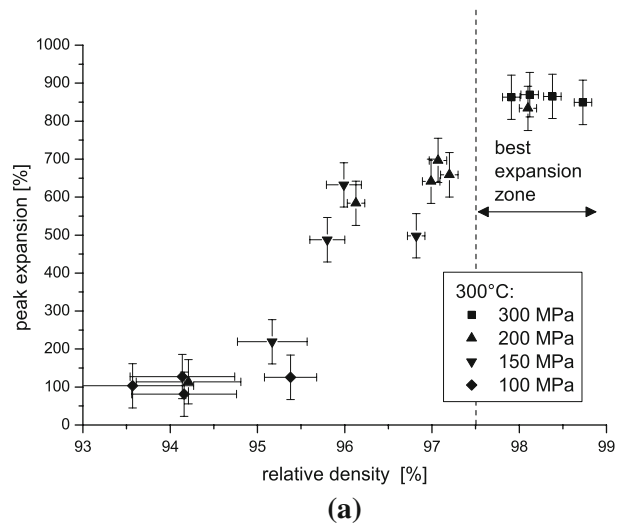
Fig. 6—Peak expansion for precursors compacted at (a) 300 °C and (b) 400 °C at different pressures as a function of the relative density of the precursor. Pressing times vary. Values corresponding to different compaction pressures are marked by different symbols. The box A marks a group of points discussed in the text.

High compaction pressures, *i.e.*, 250 or 300 MPa, lead to a constant or decreasing peak expansion, while lower compaction pressures show a peak around 400 °C and lower expansions below this temperature.

At low compaction pressures, a minimum compaction temperature is required to gain satisfactory foam expansion. For 200 MPa, this temperature is between 250 °C and 300 °C; for 100 MPa, it is between 300 °C and 400 °C. An increase in the compaction temperature up to 450 °C leads to a decrease in the peak expansion for the highest (300 MPa) and lowest (100 MPa) compaction pressure applied. Figure 5(a) can be briefly summarized: At low pressures, a certain minimum temperature is needed to ensure good expansion; at high pressures, a temperature increase is deleterious and intermediate temperatures suffice.

In Figure 5(b), the temperature dependence of the peak expansion of precursors pressed at 250 MPa for four different compaction times is given. The result is

that an increasing compaction temperature is useful for short pressing times, *i.e.*, 30 or 90 seconds, but not for long compaction times. At 400 °C, all the expansion values are very similar again.

D. *Peak Expansion as a Function of Density*

In Figure 6, the measured peak expansion values are given as a function of the measured precursor density, for precursors compacted at 300 °C and 400 °C. Figure 6(a) shows that there is a monotonic increase in peak expansion with density. Above approximately 97.5 pct, the expansion is approximately constant at the very high level of >850 pct. The highest expansion values can be achieved at high compaction pressures (300 MPa). Still "satisfactory" expansion values can be achieved above a relative precursor density of ≈96 pct. The values of the minimum compaction pressure needed to achieve this at a 300 °C compaction temperature
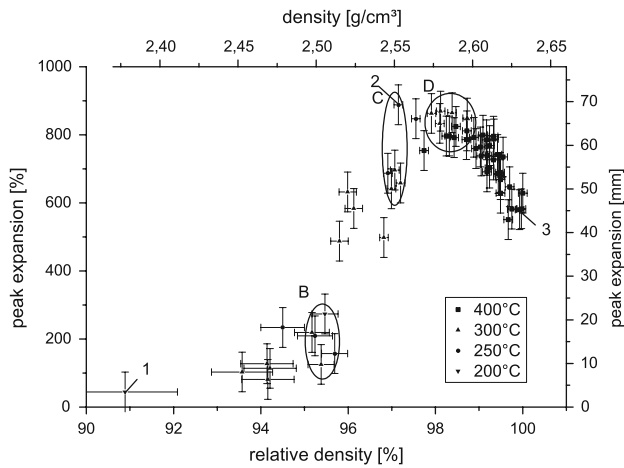
Fig. 7—Peak expansion given as a function of precursor density for four different compaction temperatures. Compaction pressures and times vary. Data points of Figs. 6(a) and (b) are included along with additional data. The samples chosen for microstructural examination are marked (1) through (3); three areas for the comparison of different parameters sets at similar precursor densities are encircled (B) through (D).

range from 150 to 200 MPa, depending on compaction time.

The peak expansion values of precursors pressed at 400 °C given in Figure 6(b) show a significant decrease with precursor densities above ≈99 pct. Such densities are reached at higher compaction pressures. At precursor densities between 99 and 99.6 pct (zone A in Figure 6(b)), higher compaction pressures lead to higher expansions when the precursor density is comparable. Even higher densities were all achieved with the highest pressure.

In Figure 7, all the peak expansion data are shown as a function of the relative precursor density. Different symbols allow us to distinguish different compaction temperatures. The correlation between the precursor density and achieved peak expansion is obvious. At a relative density of ≈98 pct, expansion values reach a maximum. Still satisfactory expansion values, *i.e.*, (≥500 pct), are reached for compaction at 250 °C, if the precursor density exceeds ≈96 pct. In the range between 94 and 98 pct relative density, the peak expansion increases from 100 to nearly 900 pct. At densities >98 pct that in most cases were achieved by pressing at 400 °C, expansion values decrease but still exceed 500 pct in all cases.

After compaction at 200 °C, the peak expansion never exceeds 300 pct, even if high values for the other two pressing parameters are chosen (900 seconds, 300 MPa). At a similar density, some further effects can be observed: The precursor compacted at 200 °C reaches an expansion higher than those of comparable density compacted at 250 °C (zone B in Figure 7). In zone C, peak expansions of precursors compacted at 250 °C exceed the expansion values of precursors compacted at 300 °C with equal or slightly higher density. Zone D shows slightly higher expansion values for a 300 °C compaction temperature than for a 400 °C.

E. *Microstructure of Precursor Material*

Three parameter sets for sample compaction were chosen for microstructural investigation. The corresponding results are marked in Figure 7 by the following numbers.

(1) Insufficient compaction: 200 MPa, 300 seconds, 200 °C. At a relative precursor density of 90.9 pct, an expansion value of just 44 pct has been reached.
(2) Optimal compaction: 300 MPa, 300 seconds, 250 °C. With 888 pct, this sample showed the highest expansion reached in this study at a relative precursor density of 97.2 pct.
(3) Overcompaction: 300 MPa, 900 seconds, 400 °C. With the high relative density of 99.8 pct, this sample reaches an expansion value of 580 pct.
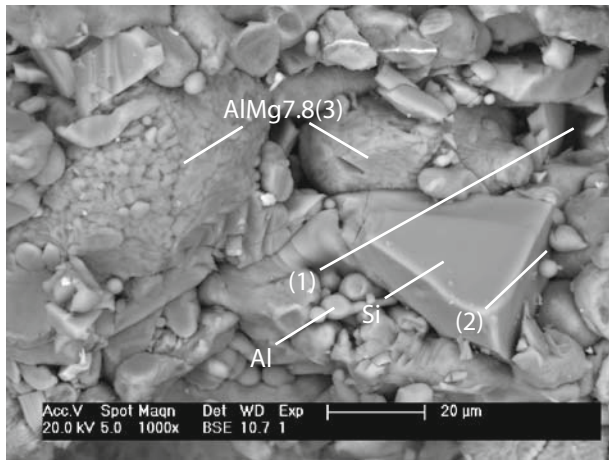
Figure 8 shows SEM micrographs of fracture surfaces. The individual particles of different types can identified. The TiH_2 particles appear brighter than the other powders; silicon has a distinct angular shape, while AlMg7.8 is much coarser than the other particles (3).

Sample 1 shows features of a loose bulk of particles. Between the particles, one can clearly identify voids (1). Particles barely show plastic deformation, which can be seen, for example, at the interface between the two Al particles adhering to a Si particle (2).

Sample 2 appears much denser. One can still identify the original particles, but the fracture surfaces reveal that like Al particles are plastically deformed and develop metallic bonding, whereas no metallic bonding between unlike particles is observed. One can see this at the concave imprint of an AlMg7.8 particle (4), where the borders between the formerly separated particles are still visible. Nevertheless, one can still find voids in the sample, for example, at the Si particles (5), although in general, the plastic deformation of the Al levels out shape differences, *e.g.*, at the imprint of the corner of a silicon particle, partially broken out of the materials' surface (6).

The fracture surface of sample 3 shows a structure similar to sample 2. One can see the good shape-fitting between the Si particles and the deformed Al matrix at (7). The concave zone in the lower part of the image (8) is similar to the imprint found in sample 2 (4), a previous border between softer Al and one hard AlMg7.8 particle, indicating that particle bonding between Al and AlMg7.8 is weaker than Al-Al bonding. In the valleys of the fracture surface, one can see many small voids that appear as narrow gaps (9). Figure 9 shows the ground surfaces of the three samples. Sample 1 shows pores with a cross section of up to 176 μm^2 (1). Those appear preferentially, but not exclusively, next to Si particles. In all samples, plenty of pores with a cross section of just a few micrometers (2) can be found. The larger pores in sample 1 (1) are significantly different than the smaller pores in shape (2). While the small pores are nearly round, the large pores appear as elongated gaps.
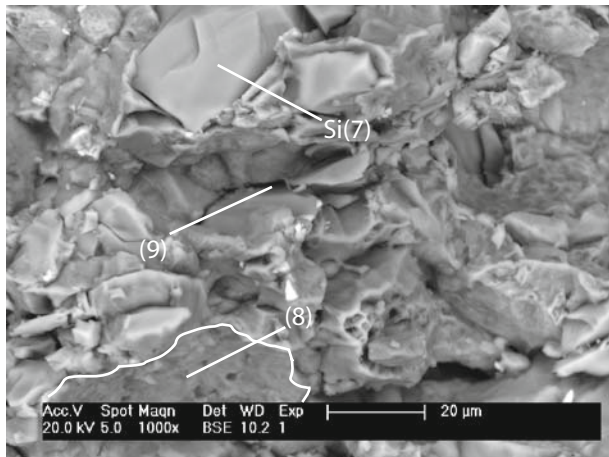
Samples 2 and 3 show none of those very large gaplike voids, but small pores appear in high numbers. The ones
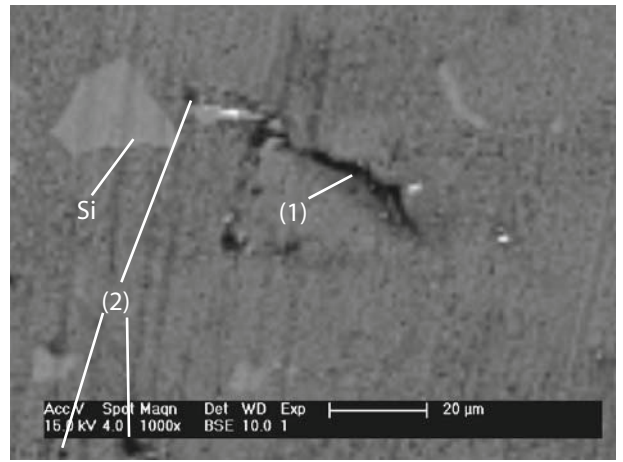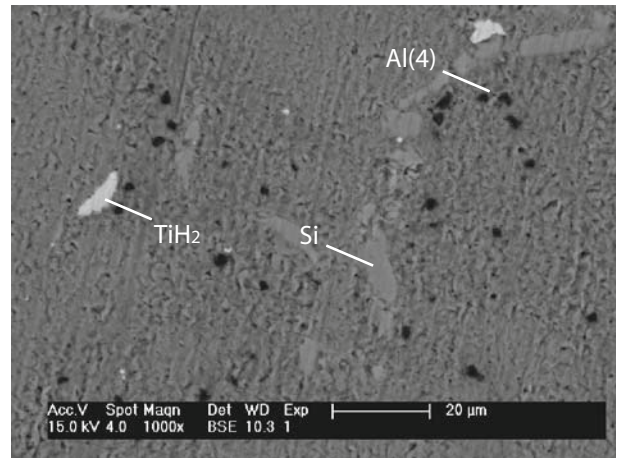
(a)

(b)

(c)

(a)
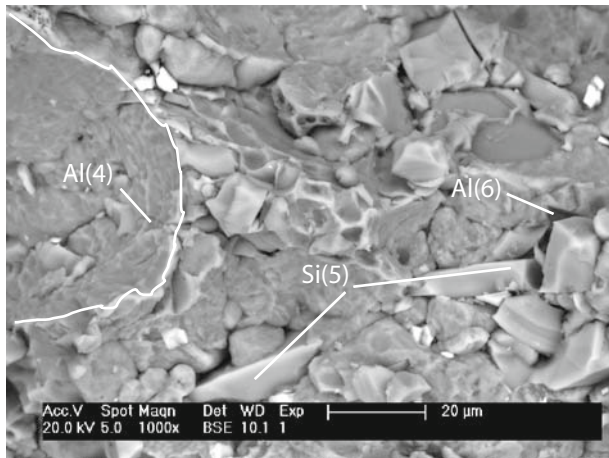
(b)

(c)

Fig. 8—SEM micrographs of fracture surfaces for precursors compacted in different ways: (*a*) 200 MPa, 300 s, 200 °C; (*b*) 300 MPa, 300 s, 250 °C; and (*c*) 300 MPa, 900 s, 400 °C. Compaction direction is from top to bottom. The marks (1) through (9) are discussed in the text.

Fig. 9—SEM micrographs of ground precursor samples. Same states as in Fig. 8, namely: (*a*) 200 MPa, 300 s, 200 °C; (*b*) 300 MPa, 300 s, 250 °C;, and (*c*) 300 MPa, 900 s, 400 °C. Compaction direction is from top to bottom. Marks (1) through (6) are discussed in the text.
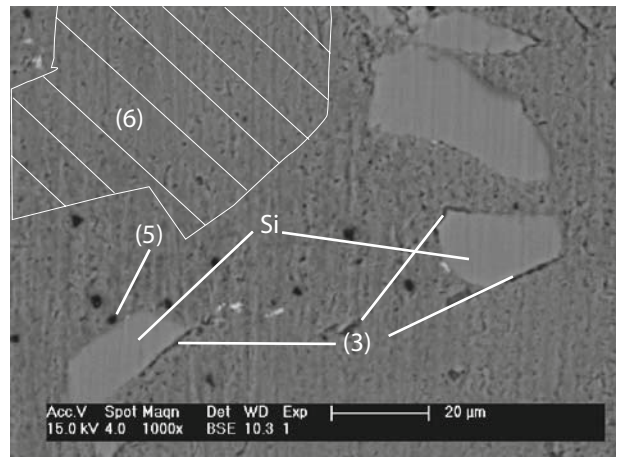
appearing next to the Si particles (3) are smaller than the corresponding ones in sample 1. The finely spread porosity shows the tendency of the pores to concentrate

preferentially in some particular areas (4), with just a few micrometers' distance between the particular pores, indicating the location of former particle boundaries.
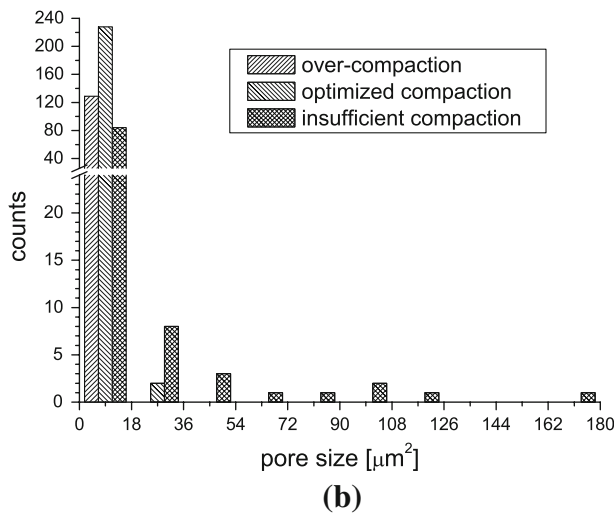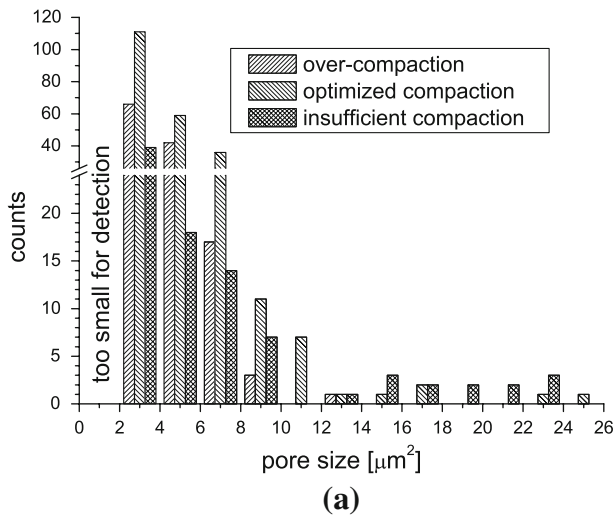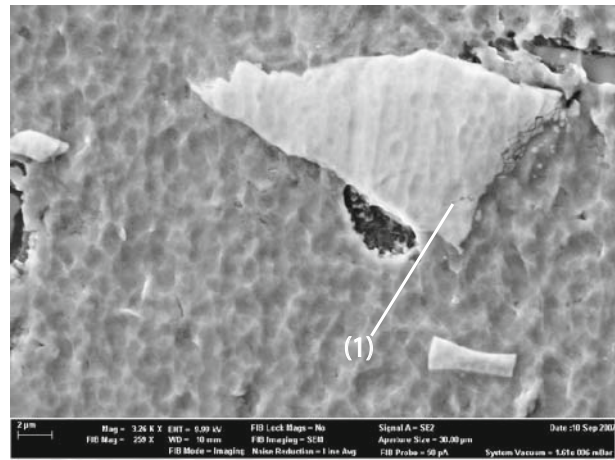
Fig. 10—(a) Histogram of the pore size distribution of the detected pores up to a 26-μm^2 cross section and (b) the histogram containing all identified pores gained from SEM images.

Fig. 11—High-resolution SEM images of embedded TiH$_2$ particles for two of the compaction states: samples (a) 3 and (b) 1. Compaction direction is from top to bottom; marks are discussed in the text.
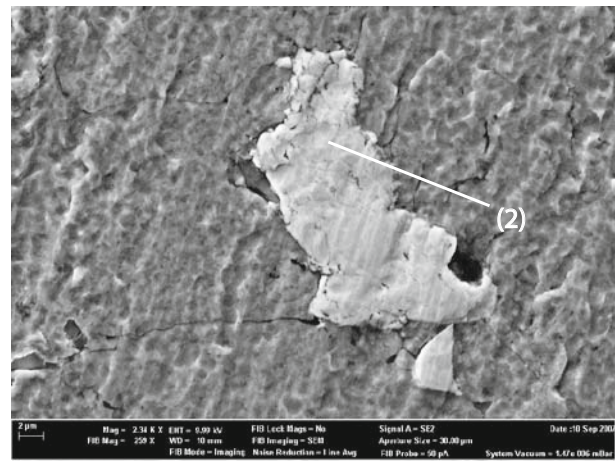
Sample 3 shows qualitatively the same finely spread porosity as sample 2, but clearly in lower numbers. The pores can be also found in the consolidation zones between the Al particles (5). Although AlMg7.8 particles are difficult to identify, they appear as pore-free areas (6). Voids at the Si particle borders (3) are even smaller than in sample 1, but the shape difference between Al-Si (3) and Al-Al (2,4,5) voids is obvious.

The results of the image analysis performed on lower-magnification images than those shown in Figure 9 are given in Figure 10. The smallest measured cross section necessary for the identification is $\approx 3~\mu m^2$ (4 pixels). The total analyzed area of an image is 27,000 μm^2. For small pores with a size near the detection limit, the measured area is very much higher than the physical cross section, due to the fact that pixels partly covered by the physical pore are completely counted as pore area.

In Figure 10(b), one can see the main difference between sample 1 and the other samples; sample 1 is the only one showing pores with high cross sections up to 180 μm^2. Fully 95 pct of the pores are smaller than

67 μm^2, while for samples 2 and 3, these limits are just 11 and 7 μm^2, respectively. The measured overall porosity is highest for sample 1, where 60 pct of the total area is found in pores larger than 26 μm^2.

In order to examine the fracture behavior of TiH$_2$ particles during pressing, ion-milled surfaces of the samples were examined by a high-resolution SEM. The damage in the TiH$_2$ particles ranges from single cracks ((1) in Figure 11(a)) to nearly completely fragmented particles ((2) in Figure 11(b)), and is visible in all the samples. The width of the cracks normally does not exceed 1 μm; for most cracks, it is $\approx$100 nm.

IV. DISCUSSION

A. Comparison to Other Studies

We shall first discuss some data available in the literature. Duarte and Banhart[5] studied an AlSi7 alloy containing 0.6 mass pct of untreated TiH$_2$. The compaction temperature was varied between 200 °C and 550 °C at a constant compaction pressure of 112 MPa.

At relative precursor densities of around 99 pct, the highest expansions, ranging up to ≈520 pct, are achieved. For 96.3 and 97.3 pct density, expansions are lower but show an increasing tendency, which fits qualitatively to our results (Figure 7). At 91.8 pct density, the precursor is reported to be virtually unfoamable. For 400 °C and 450 °C, an equally high peak expansion of 520 pct is found. A massive loss of expansion ability is observed at temperatures approaching 550 °C.

In this study, we found the expansion maximum at comparable compaction pressures (100 MPa) at ≈400 °C (Figure 5(a)). Already at 450 °C, we observe a notable decrease in the peak expansion to approximately 500 pct. Therefore, the precursors in Duarte's study tolerate higher pressing temperatures without losing much of their foamability. Compaction time plays a minor role both in Reference 5 and in the present study, if compaction pressures around 100 MPa are applied. The loss of foaming capacity is explained by gas losses during pressing in Reference 5. Because the maximum of foamability is found at lower temperatures in the present study, although TiH_2 pretreated in air at 480 °C for 3 hours has been used whereas Duarte uses untreated powder that decomposes at lower temperatures, the loss of foamability for higher pressing temperatures cannot be explained by this mechanism only. The generally smaller expansion ratio of Al-Si alloys compared with the Al-Si-Mg alloy used in this study is caused by the difference in the melting ranges and the associated different kinetics of the blowing-agent decomposition, aside from other factors such as the melt rheology.

Kennedy et al. study the densities of cold-compacted pure aluminum powders containing 1 mass pct TiH_2 and their foaming behavior.[20] Compaction pressures range up to 655 MPa. With increasing pressure, a first foam expansion of merely 11 pct is observed for precursors having a 92.2 pct relative density (pressed at 310 MPa). A pronounced increase in expansion to 214 pct is seen when the precursor density is 97.1 pct, after which a further density increase to 99.1 pct yields a peak expansion of 256 pct. If we take into account that pure aluminum foams expand less in general and that the blowing agent had a different pretreatment, these results are in good agreement with ours. We could not achieve foaming by the cold compaction of AlSi8Mg4, because the pressure required probably exceeds the maximum pressure range we could apply. An interesting point is that, in Reference 20, the amount of interconnected (open) porosity was measured. It was observed that the closing of the interconnected pore system roughly coincides with the increase in foamability.

Asavavisithchai and Kennedy study the influence of the compaction temperature and preoxidation of the used powders on foam expansion.[13,21] A compaction pressure of 150 MPa and pressing temperatures from 400 °C to 550 °C were used. Pure aluminum (99.7 pct) was used, with 0.6 mass pct TiH_2 as the blowing agent. Precursor densities are given as a >99 pct relative density; compaction time is not mentioned.

In the range of their hot-compaction parameters corresponding to the ones applied in our study, reported peak expansions show no influences exceeding the experimental scatter reported to be ±20 pct. The reported expansions are, in any case, quite low (≈350 pct), due to the pure aluminum used, making quantitative comparison of the results with our study difficult, because the effects we observed with similar compaction parameters showed up at much higher expansion values (≥500 pct).

Cold compaction is found to yield foam while, in our study, samples compacted at 200 °C were nearly unfoamable. One has to take into account that the higher compaction pressure used for cold compaction (650 MPa), combined with the softer metal, leads to densities that always resulted in good expansions in our study.

B. Results of Present Study

The parameters pressure, time, and temperature all had an influence on the density of the pressed precursor. Within the experimental error, the correlation between the density and one of the pressing parameters is always positive, similar to the dependence shown in Figure 1. Because this is almost trivial, these results were not shown. It is possible to achieve densities close to a fully dense material. Nevertheless, even in the densest samples, a small amount of microporosity is found (Figures 8 and 11).

In contrast to the precursor density, the peak expansion during foaming is not correlated with any of the three pressing parameters in a simple way. For example, a monotonic dependence of the peak expansion on compaction time can be found at just 300 °C and moderate compaction pressures (Figure 3(a)). The compaction pressure has a positive influence at a 300 °C compaction temperature (Figure 4(a)), but leads to a slight expansion decrease at 400 °C (Figure 4(b)). For the compaction temperature, it turned out more clearly that optimum values exist depending on the other parameters (Figure 5).

The clear dependence of the peak expansion on the relative precursor density, as displayed in Figures 6 and 7, shows that the porosity in the precursor plays an important role. On the low-density side, an increase in the relative precursor density up to ≈98 pct leads to an increase in peak expansion. This is understandable and has been discussed in the literature[5] as the effect of the decreasing interconnectivity of the pores that can lead to hydrogen losses during heating. The SEM observations of the fracture surfaces displayed in Figure 8 show that, for insufficient densification, there is little metallic bonding between particles, leaving thin channels interconnecting the porosity.

The processes taking place during compaction of the precursor are schematically illustrated in Figure 12. In the loose powder, porosity is coarse and interconnected (Figure 12(a)). In the schematic diagram (Figure 12(e)) of the porosity development, this corresponds to the initial state at >40 pct total porosity that exists as a volume fraction Θi of interconnected porosity only.
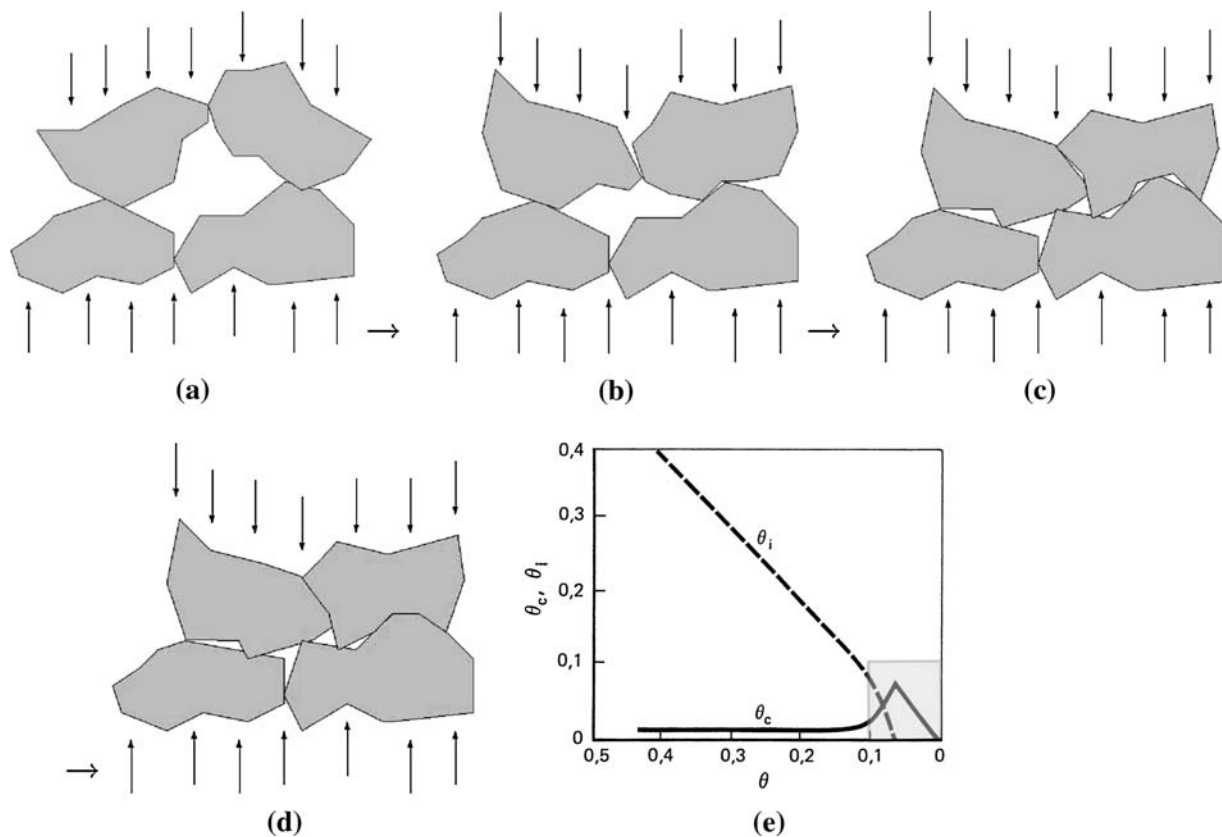
Fig. 12—(a) through (d) Schematic illustration of particle rearrangements during compaction and (e) the development of the interconnected Θi and closed porosity Θc as a function of overall porosity Θ during hot compaction (taken from Ref. 22). The density range considered in Fig. 7 has been shaded.

When compaction starts, a second type of smaller closed pores with a volume fraction Θc develops between the particles (Figure 12(b)). The Θc remains on a very low level until the very late stages of densification ($\Theta \approx 12$ pct in this diagram). With proceeding densification, the closure of interconnected pores generates an increasing amount Θc of closed porosity. After the densification process has reached a residual porosity of ≈ 6 pct, the interconnected porosity has completely disappeared, and $\Theta i \approx 0$ (Figure 12(d)). This is very roughly the stage at which the pressed powder precursors start to become foamable. Even further densification eventually reduces the volume of the closed pores and the corresponding peak expansion increases simultaneously up to a 99 pct precursor density.

It is surprising that, as densification exceeds 99 pct, relative precursor density peak expansion decreases again. At a 400 °C compaction temperature, at which these high densities can be prepared, this effect can be observed to depend on a combination of increasing compaction time and pressure, but cannot be assigned to just one single parameter. The effect has not been described before in the literature.

As possible reasons for the at-first-sight counterintuitive decrease in the peak expansion with density, five possible explanations will be discussed in the following.

1. *Hydrogen losses during compaction*

The higher temperatures used for achieving the highest precursor densities could lead to the decomposition of the blowing agent already during pressing and therefore negatively affect peak expansion. Untreated TiH_2 powder starts to decompose at 380 °C,[8] but the released amount of gas is low up to approximately 400 °C, after which it peaks at 540 °C. This may lead to significant hydrogen losses for the high compaction temperatures studied in the literature.[5,13,21] In the present case, however, the TiH_2 powder used has been heat treated under air at 480 °C for 3 hours, leading to a much higher onset temperature of decomposition of ≈ 500 °C.[8] Therefore, it seems unlikely that such gas losses can have an adverse effect on peak expansion at 400 °C.

2. *Fracture of TiH_2 particles*

Blowing-agent particles embedded in a metallic matrix (or milled powders) release gas at lower temperatures than does loose untreated powder.[5,23–25] This also holds for preoxidized powders when the decomposition kinetics of loose powders are compared to the ones of PM precursors[8] and has been explained by the mechanical fracture of individual blowing-agent particles during compaction, the associated breaking of oxide skins, and the correspondingly shorter diffusion

pathways of the hydrogen atoms to the surface of the TiH$_2$ particles.

We found cracked TiH$_2$ particles in all samples observed with a SEM (Figure 11). The $\approx$100-nm-thick oxide layers were not examined, because this requires a transmission electron microscope.[8] Because severe damage is observed for all three compaction conditions (including condition 2, representing best foaming), there is no evidence that stronger compaction would exacerbate this effect and lead to stronger gas losses.

The softening of the TiH$_2$ and its oxide layer is minor compared to that of aluminum in the temperature range up to 400 °C. Therefore, one would expect most of the cracking of the TiH$_2$ particles would occur during cold precompaction rather than during hot compaction, because both were performed at the same compaction pressure. This is confirmed by the SEM images in Figure 11, which show brittle fracture of the TiH$_2$ particles. The fracture surfaces shown in Figure 8 confirm that TiH$_2$ is not deformed. Due to this, the key parameter for mechanical damage of the TiH$_2$ particles is the compaction pressure. In Figure 6(b), the compaction pressure shows a slight positive influence on peak expansion at comparable densities >99 pct and a 400 °C compaction temperature. Furthermore, at this temperature, the decrease in peak expansion with density does not depend on the compaction pressure alone, but also on the compaction time. For these reasons, the influence of the compaction-induced fracture of the TiH$_2$ particles is unlikely.

3. *Oxidation of metal particles*

During compaction, both the individual aluminum and the AlMg7.8 particles could be oxidized, because the pressing die was not sealed. This could lead to insufficient bonding between particles and could contribute to hydrogen losses and, therefore, decrease peak expansion. Furthermore, due to the higher density of alumina as compared to aluminum, the oxidized sample would have a higher relative density. One could suspect that the measured higher densities at a 400 °C compaction temperature are caused by weight gain due to oxidation during hot compaction or by densification. The quantitative data for the influence of oxide content on precursor density can be obtained from Figure 1. Such an effect is considered unlikely, due to several observations: (1) the SEM images show a decrease in the residual microporosity from samples 2 to 3, (2) Asavavisithchai and Kennedy reported that there is no oxide formation in pure aluminum powder mixtures at 400 °C,[13,21] and (3) longer compaction times should lead to more oxide formation. In contrast, higher compaction pressures should suppress oxide formation, because better precompaction prevents air from entering the compact. However, only at the highest compaction pressure would a longer compaction time reduce the peak expansion (Figure 3(b)), whereas for the lower compaction pressure, time has no influence. If oxidation was the reason for the reduction of peak expansion, this phenomenon should be more pronounced for low compaction pressures, at which air has more access to the interior of a tablet (Figure 6(b)).

4. *Air inclusions*

During hot compaction, the air entrapped in closed pores could reach such high pressures that the metallic matrix after pressing would crack. During subsequent foaming, blowing gas could partially escape through these cracks.

To discuss this possibility, an estimate for the pressure inside the closed porosity is required. During precompaction of the powder and perhaps even in early compaction stages, most of the porosity is still interconnected and the entrapped gas would be in a pressure equilibrium with the ambient. In the course of further densification, the air gets encapsulated in the now increasingly closed porosity (Figure 12(e)). This is expected to happen above a $\approx$90 pct relative density.

As the relative density rises from 90 to 99 or even 99.9 pct, the pressure in the micropores shown in detail in Figure 11(a) rises from 0.1 to 1 or 10 MPa, respectively, if the air is treated as ideal gas.

Because aluminum at 400 °C has largely softened, such overpressures could lead to interparticle cracking after unloading of the die. The cracks created could facilitate hydrogen losses.

5. *Influence of Microporosity*

Because for a more than 99 pct precursor density both the peak expansion and residual closed porosity decrease, it is worth considering that there is a correlation between the two. Here, we assume that residual compaction pores act as nucleation centers for bubble formation during foaming.

The diffusion of hydrogen in aluminum or other metals, especially heterogeneous ones such as powder compacts, is influenced by microstructural heterogeneities. The reported diffusion coefficients show a large scatter[26] due to microstructural features. For foamable precursors, we can assume a large diffusivity due to the presence of a high number of fast diffusion routes in the compacted material. Hydrogen gas has the tendency to accumulate in small voids (trapping). Those hydrogen filled traps can expand to pores as the surrounding metal melts. This assumption is justified by the results of neutron scattering experiments performed on zinc foams.[27] The existence of an initial porosity with a pore size in the order of magnitude of the residual porosity after compaction observed in this study is reported. Furthermore, it is reported that this porosity completely disappears in the foaming process during the early stages of pore formation, at $\approx$10 pct porosity.

We could quantify by image analysis that there is a decrease in the level of residual microporosity and a corresponding lower number of nucleated pores. This means that, at the same coalescence rate, a higher volume expansion can be achieved before the pores reach a pore size, making the foam unstable. The pathway to higher densification appears unimportant, because all values collapse on the same line in Figure 7. This explanation is compatible not only with the results of the present study but also with the literature.[5,13,21]

In summary, the observed drop in the peak expansion could be a combination of a too-low level of nucleation centers and, possibly, cracks in the precursors that open

during the foaming process. Of course, all these findings refer to the specific alloy studied. Preliminary studies show that there is no such effect in pure aluminum.[28]

C. Selection of Compaction Parameter for Production

For metal foam production, the appropriate choice of parameters for powder compaction is essential and the present study can provide guidelines. The specific values for the compaction parameters have to be determined for the alloy composition used. The details most likely also depend on the type of the powders. A paramount criterion for high foam expansion is the precursor density; different parameter sets such as (300 °C, 300 MPa, 900 seconds) and (400 °C, 150 MPa, 100 seconds) are nearly equivalent in terms of foaming. The parameters chosen have to ensure merely that a relative precursor density of ≥97.5 pct is achieved. Therefore, there is some flexibility in selecting the best parameters for high cost efficiency. Further boundary conditions that prevent us from applying "exotic" parameters are the thermal stability of the blowing agent and the lifetime of the pressing tool.

Uniaxial pressing is a simple and flexible method of manufacturing small pieces of precursor material and is the preferred compaction method for research. Still, for the mass production of foamable precursors, methods such as powder rolling[29] or extrusion are preferred. Small parts, such as the energy absorber for the Audi† Q7

---

†Audi is a trademark of AUDI AG, Ingolstadt, Germany.

---

vehicle,[30] are produced by cutting small pieces off a long rod of extruded material. As an alternative, one would hot press small parts of a precursor to be foamed in a die without further processing. Because compaction time can be radically shortened down to values of 1 second if the other parameters are chosen sufficiently high (Figure 3(b)), hot pressing could be an option for mass production. One problem associated with the hot pressing of a high number of pieces is that of tool wear. Aluminum powder tends to stick to tool steels and eventually degrade their surfaces unless proper protection measures are taken.

V. SUMMARY AND CONCLUSIONS

The conclusions that can be drawn from this study are the following.

1. Increasing compaction time, pressure, or temperature lead to higher precursor densities.
2. In the case of the powder mixture we used, densification sufficient for high expansion can be reached for compaction temperatures of 250 °C and above.
3. For lower temperatures, the compaction pressure has a stronger influence on expansion than for higher temperatures.
4. Compaction time can be shortened to 1 second if the other parameters that are chosen are high enough.

5. Peak expansion clearly depends on precursor density. The parameter set that leads to a specific density is of secondary importance.
6. The minimum relative density needed for "satisfactory expansion" is ≈96 pct, whereas densities between 97.5 and 99 pct lead to the highest foam expansions (880 pct in the present case).
7. Densities that are too high (≥99 pct) have an adverse effect on foam expansion in this alloy and powder system.
8. Most likely, the loss of pore nucleation centers and cracks created by the high pressure of the entrapped and compressed air in the residual porosity are the reasons for this unexpected and never previously reported effect.

REFERENCES

1. B.C. Allenand, M.W. Mote, and A.M. Sabroff: U.S. Patent No. 3,087,807, 1959.
2. J. Baumeister: German Patent No. DE 4018360 C1, 1990.
3. F. Baumgärtner, I. Duarte, and J. Banhart: *Adv. Eng. Mater.*, 2000, vol. 2, pp. 168–74.
4. L.-P. Lefebvre, J. Banhart, and D.C. Dunand: *Adv. Eng. Mater.*, 2008, vol. 10, pp. 775–87.
5. I. Duarte and J. Banhart: *Acta Mater.*, 2000, vol. 48, pp. 2349–62.
6. F. Garcia-Moreno, M. Fromme, and J. Banhart: *Adv. Eng. Mater.*, 2004, vol. 6, pp. 416–20.
7. D. Lehmhus and G. Rausch: *Adv. Eng. Mater.*, 2004, vol. 6, pp. 313–30.
8. B. Matijasevic, J. Banhart, S. Fiechter, O. Görke, and N. Wanderka: *Acta Mater.*, 2006, vol. 8, pp. 864–69.
9. D. Lehmhus and M. Busse: *Adv. Eng. Mater.*, 2004, vol. 6, pp. 391–96.
10. H.-M. Helwig: Doctoral Thesis, Technische Universität Berlin, Berlin, 2009, submitted.
11. C. Körner, F. Berger, M. Arnold, C. Stadelmann, and R.F. Singer: *Mater. Sci. Technol.*, 2000, vol. 16, pp. 781–84.
12. F. Garcia-Moreno, N. Babcsan, and J. Banhart: *Coll. Surf., A*, 2005, vol. 263, pp. 290–94.
13. S. Asavavisithchai and A.R. Kennedy: *Adv. Eng. Mater.*, 2006, vol. 8, pp. 810–15.
14. L. Bonaccorsi and E. Proverbio: *Adv. Eng. Mater.*, 2006, vol. 8, pp. 864–69.
15. J. Banhart and H.-W. Seeliger: *Adv. Eng. Mater.*, 2008, vol. 10, pp. 793–802.
16. *Kenndaten von Werkzeugstählen–ORVAR SUPREME Warmarbeitsstahl*, Boehler-Uddeholm GmbH, Düsseldorf, 1998, 12 pp.
17. H.-M. Helwig and J. Banhart: in *Cellular Metals and Metal Foaming Technology*, J. Banhart, M.F. Ashby, and N.A. Fleck, eds., MIT - Verlag, Berlin, Germany, 2003, pp. 165–68.
18. University of Texas Health Science Center, home page of UTHSCSA ImageTool, http://ddsdx.uthscsa.edu/dig/itdesc.html.
19. A. Dudka, F. Garcia-Moreno, N. Wanderka, and J. Banhart: *Acta Mater.*, 2008, vol. 56, pp. 3990–4001.
20. A.R. Kennedy and S. Asavavisithchai: *Mater. Sci. Forum*, 2002, vols. 396–402, pp. 251–58.
21. A. Kennedy and S. Asavavisithchai: in *Porous Metals and Metal Foaming Technology*, H. Nakajima and N. Kanetake, eds., The Japanese Institute of Metals (JIM), Sendai, Japan, 2005, pp. 139–44.
22. W. Schatt: *Sintervorgänge*, VDI-Verlag, Düsseldorf, Germany, 1992.
23. F. von Zeppelin, M. Hirscher, H. Stanzick, and J. Banhart: *Compos. Sci. Technol.*, 2003, vol. 63, pp. 2293–2300.
24. V. Bohsle, E.G. Baburaj, M. Miranova, and K. Salama: *Mater. Sci. Eng., A*, 2003, vol. A356, pp. 190–99.
25. A. Ibrahim, C. Körner, and R.F. Singer: *Adv. Eng. Mater.*, 2008, vol. 10, pp. 845–48.

26. G.A. Young and J.R. Scully: *Acta Mater*., 1998, vol. 46, pp. 6337–49.
27. J. Banhart, D. Bellmann, and H. Clemens: *Acta Mater*., 2001, vol. 49, pp. 3409–20.
28. D. Pan: Masterthesis, TU Berlin, Berlin 2009.
29. S. Vatchiants and N. Manunkyan: in *Porous Metals and Metal Foaming Technology*, H. Nakajima and N. Kanetake, eds., The Japanese Institute of Metals (JIM), Sendai, Japan, 2005, pp. 195–99.
30. P. Schaeffler, G. Hanko, H. Mitterer, and P. Zach: in *MetFoam 2007: Porous Metals and Metallic Foams*, L.P. Lefebvre, J. Banhart, and D. Dunand, eds., DEStech Publications, Inc., Lancaster, PA, 2007, pp. 7–10.